# Altered Stability and Degradation Pathway of CH<sub>3</sub>NH<sub>3</sub>PbI<sub>3</sub> in Contact with Metal Oxide

Sampreetha Thampy, <sup>a</sup> Boya Zhang, <sup>a</sup> Ki-Ha Hong, <sup>b</sup> Kyeongjae Cho, <sup>a</sup> Julia W. P. Hsu\*<sup>a</sup>

<sup>a</sup> Department of Materials Science and Engineering, University of Texas at Dallas, Richardson, TX 75080, USA.

<sup>b</sup> Department of Materials Science and Engineering, Hanbat National University, Yuseong-Gu, Daejeon, 34158, Republic of Korea.

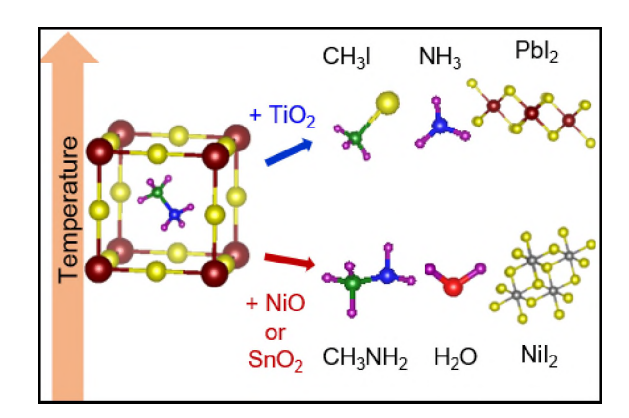
## **AUTHOR INFORMATION**

# **Corresponding Author**

\* Department of Materials Science and Engineering, University of Texas at Dallas, Richardson, TX 75080, USA. Email: jwhsu@utdallas.edu.

ABSTRACT. Degradation in CH<sub>3</sub>NH<sub>3</sub>PbI<sub>3</sub> (MAPbI<sub>3</sub>), when in contact with commonly used metal oxide transport layer materials in optoelectronic devices, is examined experimentally and theoretically. Based on the decomposition temperature, the interfacial stability decreases in the following order: MAPbI<sub>3</sub> + TiO<sub>2</sub> ~ MAPbI<sub>3</sub> alone > MAPbI<sub>3</sub> + SnO<sub>2</sub> > MAPbI<sub>3</sub> + NiO, consistent with thermodynamic data. When MAPbI<sub>3</sub> contacts NiO or SnO<sub>2</sub>, experimental results unequivocally show interfacial decomposition occurs at a lower temperature than bulk decomposition and produces different degradation products. Density functional theory calculations reveal altered reaction pathway on oxide surfaces and elucidate the difference between NiO and TiO<sub>2</sub>. These findings pinpoint the importance of understanding the interaction between halide perovskite and other materials used in a device to achieve intrinsically stable devices.

### **TOC GRAPHICS**



Organic-inorganic halide perovskites have demonstrated superior optoelectronic properties, making them great candidates in various applications.<sup>1-3</sup> In particular, perovskite solar cells (PSCs) have leapfrogged several technologies in power conversion efficiencies.<sup>4</sup> For these halide perovskite materials to become viable technologies, stability is a critical issue. Many works have examined the environmental stabilities of PSCs, in particular due to oxygen, humidity, and UV light.<sup>5</sup> To this date, only a few studies have examined the intrinsic thermal<sup>6-10</sup> and photo<sup>11-12</sup> stability of organic-inorganic halide perovskites. Degradation of CH<sub>3</sub>NH<sub>3</sub>PbI<sub>3</sub> (MAPbI<sub>3</sub>) by itself can proceed in two paths:

$$CH_3NH_3PbI_3(s) = PbI_2(s) + HI(g) + CH_3NH_2(g)$$
 (1)

or 
$$CH_3NH_3PbI_3(s) = PbI_2(s) + CH_3I(g) + NH_3(g)$$
. (2)

Both reactions are endothermic with approximately the same entropic contributions, with reaction (2) favored thermodynamically. <sup>8,10</sup> Experimental results depend on ambient conditions: in vacuum, release of HI + CH<sub>3</sub>NH<sub>2</sub> (reaction (1)) is observed at low temeparture, <sup>11-13</sup> but reaction (2) is reported for experiments performed under inert carrier gas at high temperatures and atmospheric pressure. <sup>6,9,14</sup> Furthermore, reaction (1) is believed to be reversible, while reaction (2) is irreversible and the true degradation pathway. <sup>12</sup> Because the bulk degradation temperature of MAPbI<sub>3</sub> or CH<sub>3</sub>NH<sub>3</sub>I (MAI) is > 250 °C, <sup>6,9</sup> above the typical processing temperature of PSCs, the intrinsic degradation studies have garnered less attention from researchers than environmental effects. However, even at low temperatures, thermodynamically driven reactions still take place, albeit at a slower rate. The temperature of gas release onset indicates the material's stability.

To date the intrinsic stability studies focused on the degradation mechanism of halide perovskites by themselves, i.e. bulk decomposition. However, in devices, the halide perovskite is in contact with other materials. For example, NiO has been used as the hole transport layer in

both solar cells and LEDs.<sup>15,16</sup> TiO<sub>2</sub> and SnO<sub>2</sub> are widely used as the electron transport layer in PSCs.<sup>17</sup> Reactions between MAPbI<sub>3</sub> and oxides have been reported previously,<sup>18-20</sup> with a recent report of MAI reacting with NiO as low as 120 °C.<sup>20</sup> With improved packaging the detriment of environment can be greatly reduced, but the interactions between halide perovskites and contact materials cannot be eliminated as contact layers are integral to the devices. Thus, understanding possible reactions from interfacial interaction is critical to address the *intrinsic* stability of perovskite devices.

In this study, the thermal stability and degradation pathways in MAPbI<sub>3</sub> and MAI, when in contact with NiO, TiO<sub>2</sub>, or SnO<sub>2</sub>, are examined using a combined temperature programmed desorption-mass spectrometry-Fourier transform infrared spectroscopy (TPD-MS-FTIR) technique. The simultaneous MS and FTIR measurements are essential for unambiguous identification of evolved gases, because MS detects ions and are complicated by ionization and fragmentation probabilities while FTIR measures the characteristic vibrational frequencies associated with specific moieties in neutral molecules, but often exhibits similar or overlapping spectra. The experimental results are augmented by thermodynamic calculations and density functional theory (DFT) modelling. The experimental and computational methodology are described in Supporting Information.

We first compare the thermal stability and decomposition pathway in pure phase MAPbI<sub>3</sub> powders<sup>21</sup> (Figure S1) to MAPbI<sub>3</sub> mixed with NiO, TiO<sub>2</sub>, or SnO<sub>2</sub> nanoparticles. Dry powders are used to avoid effects due to complexing with solvents.<sup>7,14</sup> The powder samples also accentuate the interfacial decomposition pathway (Table S1). The TPD was performed in flowing He gas (30 sccm, 760 Torr) to minimize exposure to oxygen or water vapor, i.e. environmental effects. Figure 1a shows the two-dimensional (2D) contour plots of FTIR results:

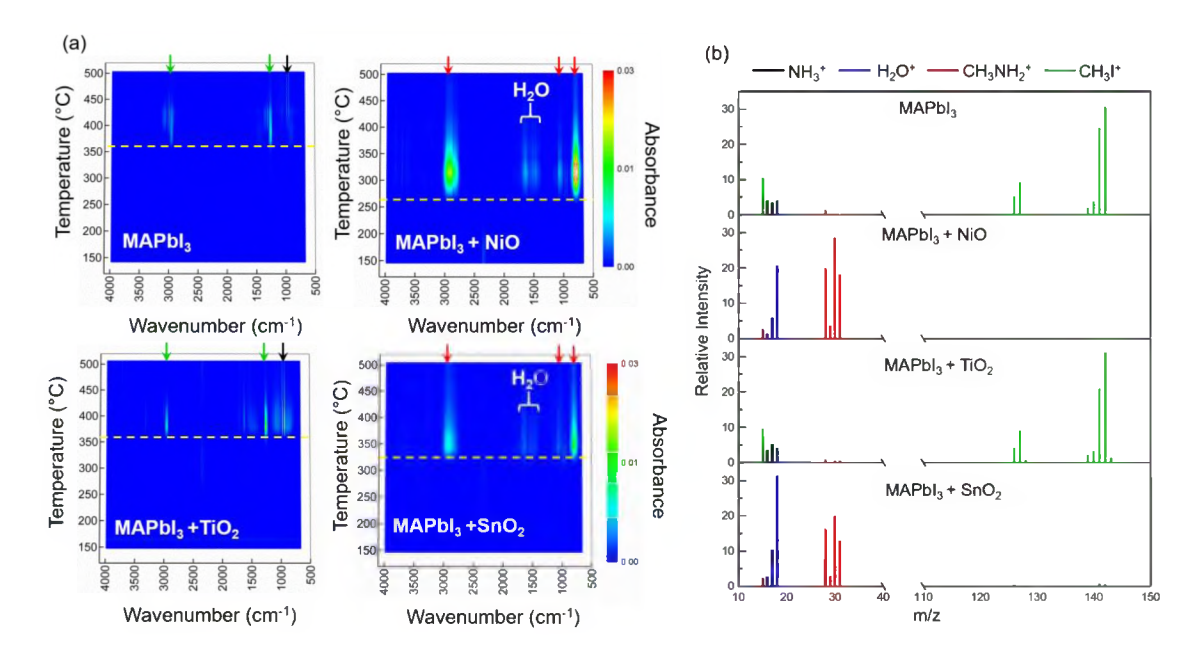


**Figure 1.** TPD-MS-FTIR results. (a) 2D contour plots of FTIR spectra (T vs wavenumber with color contours representing absorbance) for MAPbI<sub>3</sub>, MAPbI<sub>3</sub> + NiO, MAPbI<sub>3</sub> + TiO<sub>2</sub>, and MAPbI<sub>3</sub> + SnO<sub>2</sub>. The characteristic vibrational frequencies of NH<sub>3</sub>, CH<sub>3</sub>NH<sub>2</sub>, and CH<sub>3</sub>I gases are marked with black, red, and green arrows, respectively, and H<sub>2</sub>O region is marked in white. Yellow dashed lines indicate T<sub>th</sub>. (b) MS signals with NH<sub>3</sub> (black), H<sub>2</sub>O (blue), CH<sub>3</sub>NH<sub>2</sub> (red), and CH<sub>3</sub>I (green) for the 4 cases in (a). All assignments are based on NIST database.<sup>22</sup>

infrared absorbance (color scale) vs. wavenumber (x-axis) at different temperatures (T, y-axis), for neat MAPbI<sub>3</sub>, MAPbI<sub>3</sub> + NiO, MAPbI<sub>3</sub> + TiO<sub>2</sub>, and MAPbI<sub>3</sub> + SnO<sub>2</sub> (all with molar ratio 1:1). The characteristic vibrational frequencies of evolved gases during decomposition are compared to NIST database,  $^{22}$  and are assigned to NH<sub>3</sub> (black arrow), CH<sub>3</sub>NH<sub>2</sub> (red arrows), CH<sub>3</sub>I (green arrows), and H<sub>2</sub>O (white, marked in the plot). Note that for MAPbI<sub>3</sub> alone, the threshold temperature at which gases begin to evolve (T<sub>th</sub>) is  $\sim 365$  °C, which corresponds to the onset of weight loss observed at 310 °C in thermogravimetric analysis (TGA, Figure S2, black). When MAPbI<sub>3</sub> is mixed with NiO, it is clear that gases begin to evolve at  $\sim 270$  °C,  $\sim 95$  °C lower, while there is no significant change in T<sub>th</sub> when mixed with TiO<sub>2</sub> (370 °C) and a small reduction with SnO<sub>2</sub> (T<sub>th</sub>  $\sim 320$  °C). The FTIR spectra at the temperature with maximum signals

are shown in Figure S3. Figure 1b shows MS results (total gas output over the entire temperature range) for the four cases, with evolved gases identified by their mass to charge ratio (m/z) according to NIST database<sup>22</sup> and summarized in Table S2. The TPD profiles for the four cases are shown in Figure S4. For neat MAPbI<sub>3</sub>, both FTIR and MS detected only NH<sub>3</sub> and CH<sub>3</sub>I, suggesting that the bulk decomposition proceeds through the reverse N-methylation reaction<sup>6,23</sup> (reaction (2)). However, when MAPbI<sub>3</sub> is mixed with NiO, H<sub>2</sub>O and CH<sub>3</sub>NH<sub>2</sub> become the decomposition products, signaling a completely different degradation pathway, i.e. acidic hydrolysis reaction. When mixing with TiO<sub>2</sub>, MAPbI<sub>3</sub> decomposition produces the same gases as neat MAPbI<sub>3</sub>, but when mixing with SnO<sub>2</sub>, the decomposition products are the same as MAPbI<sub>3</sub> + NiO, albeit the T<sub>th</sub> is ~ 50 °C higher. The excellent agreements between FTIR and MS provide unambiguous evidence that the degradation pathway can be altered when MAPbI<sub>3</sub> is in contact with metal oxides, and depends on the metal oxides. The lower reaction temperature at the MAPbI<sub>3</sub>/NiO interface indicates lower intrinsic stability of devices when NiO is used.

To understand these experimental results, we perform thermodynamic free energy calculations based on the reaction suggested in Ref. 20. They presented that water vapor and nickel(II) iodide could be produced by the hydrogen iodide reaction with the NiO:

$$\frac{1}{2}$$
 NiO(s) + HI(g) =  $\frac{1}{2}$  NiI<sub>2</sub>(s) +  $\frac{1}{2}$  H<sub>2</sub>O(g)

By combining the above equation with equation (1), we obtain

$$CH_3NH_3PbI_3(s) + \frac{1}{2}NiO(s) = \frac{1}{2}H_2O(g) + CH_3NH_2(g) + PbI_2(s) + \frac{1}{2}NiI_2(s),$$
 (3) a reaction now possible when MAPbI<sub>3</sub> is mixed with NiO. Similarly, when MAPbI<sub>3</sub> is mixed with TiO<sub>2</sub>, it is possible to have

$$CH_3NH_3PbI_3(s) + \frac{1}{4}TiO_2(s) = \frac{1}{2}H_2O(g) + CH_3NH_2(g) + PbI_2(s) + \frac{1}{4}TiI_4(s), \tag{4}$$
 and with SnO<sub>2</sub>, it is possible to have

$$CH_3NH_3PbI_3(s) + \frac{1}{4}SnO_2(s) = \frac{1}{2}H_2O(g) + CH_3NH_2(g) + PbI_2(s) + \frac{1}{4}SnI_4(s).$$
 (5)

Free energy change ( $\Delta G^{\circ}$ ) for reactions (1)-(5) are evaluated using values from experimental data, <sup>8</sup> NIST-JANAF Thermochemical Tables, <sup>24</sup> and Materials Project<sup>25</sup> at ambient temperature, and are compared in Table S3. For bulk decomposition of MAPbI<sub>3</sub>, reaction (2) ( $\Delta G^{\circ} = 91$  kJ/mol) is favored over reaction (1) ( $\Delta G^{\circ} = 126$  kJ/mol). Note that if reactions (3)-(5) take place, the evolved gases become H<sub>2</sub>O and CH<sub>3</sub>NH<sub>2</sub>, rather than NH<sub>3</sub> and CH<sub>3</sub>I. It is clear that reaction (3) is the most favored thermodynamically; this is because the enthalpy of NiO reacting with HI (-227 kJ/mol) is much lower than that of equivalent reaction with TiO<sub>2</sub> (-45 kJ/mol) and with SnO<sub>2</sub> (-161 kJ/mol) per unit H<sub>2</sub>O generation. Thus, when MAPbI<sub>3</sub> is mixed with NiO, reaction (3) ( $\Delta G^{\circ} = 46$  kJ/mol) is favored over the bulk degradation of neat MAPbI<sub>3</sub> (reaction (2)). But when MAPbI<sub>3</sub> is mixed with TiO<sub>2</sub>, the  $\Delta G^{\circ}$  for reaction (4) (137 kJ/mol) is much higher than reaction (2); hence, MAPbI<sub>3</sub> decomposition is unaffected by contacting TiO<sub>2</sub>. Thus, thermodynamic free energy calculations confirm the order of stability indicated by decomposition temperature in TPD-MS-FTIR results: MAPbI<sub>3</sub> + TiO<sub>2</sub> > MAPbI<sub>3</sub> + SnO<sub>2</sub> > MAPbI<sub>3</sub> + NiO.

Since none of the PbI<sub>2</sub>, metal oxides by themselves, or NiO mixed with PbI<sub>2</sub> shows any gas evolution (Figure S5), the instability of MAPbI<sub>3</sub> primarily arises from MAI decomposition. Thus, we further perform TPD-MS-FTIR experiments using MAI. To investigate the competition between bulk degradation occurring in neat MAI and interfacial degradation that happens when MAI is in contact with oxide, the molar ratio of MAI:NiO is varied from 1:0, 1:0.25, to 1:4. Figure 2a shows the 2D contour plots of FTIR spectra at different temperatures and Figure 2b shows the MS results. As the results show, MAI alone (1:0) decomposes to NH<sub>3</sub> and CH<sub>3</sub>I with a  $T_{th}$  of  $\sim$  295 °C, consistent with the onset of weight loss observed at 280 °C in TGA (Figure S6, black). With excess NiO (1:4), both techniques show the evolved gases are changed to CH<sub>3</sub>NH<sub>2</sub>

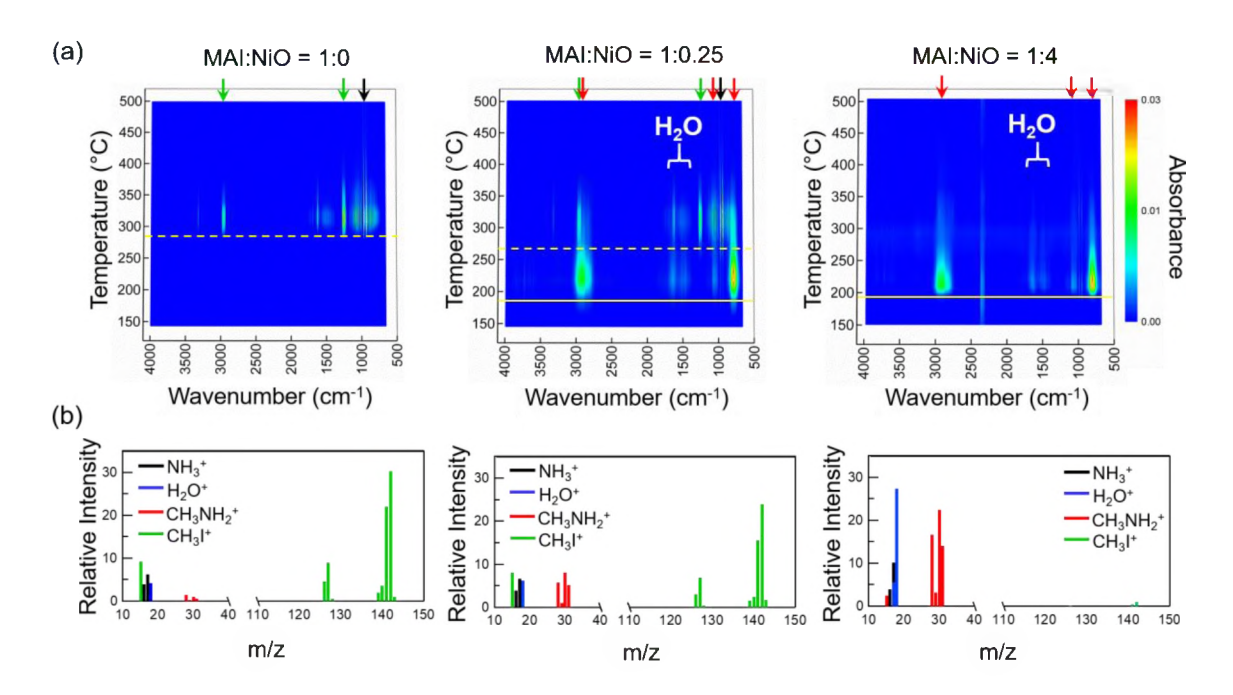


**Figure 2.** (a) 2D contour plots of FTIR spectra (T vs wavenumber with colour contours representing absorbance) for MAI:NiO with varying molar ratio of 1:0 (left), 1:0.25 (middle), and 1:4 (right). The characteristic vibrational frequencies of NH<sub>3</sub>, CH<sub>3</sub>NH<sub>2</sub>, and CH<sub>3</sub>I gases are marked with black, red, and green arrows, respectively, and H<sub>2</sub>O region is marked in white. Yellow dashed and solid lines represent T<sub>th</sub> for bulk and interfacial degradation, respectively. (b) MS signals with NH<sub>3</sub> (black), H<sub>2</sub>O (blue), and CH<sub>3</sub>NH<sub>2</sub> (red) and CH<sub>3</sub>I (green) for the 3 cases in (a). All assignments are based on NIST database.<sup>22</sup>

and  $H_2O$ , which are produced at a much lower  $T_{th}$  of ~ 200 °C. With a small amount of NiO (1:0.25), FTIR results clearly show that there are two degradation thresholds: at 190 °C (yellow solid line),  $CH_3NH_2$  and  $H_2O$  are first released, while  $NH_3$  and  $CH_3I$  only begin to evolve above 260 °C (yellow dashed line). Since the high temperature reaction occurs at the same temperature and evolved gases are the same as neat MAI, we assign this process as the bulk degradation. The low temperature process must then arise from interaction of MAI with NiO, i.e. interfacial degradation. As the amount of NiO increases, it is clear that interfacial degradation dominates over bulk degradation. The FTIR spectra at selective temperatures and MS profiles are shown in

Figure S7. In contrast, the decomposition products and T<sub>th</sub> do not vary with different amount of TiO<sub>2</sub>, as shown in Figure S8.

The similar behaviors between MAI and MAPbI<sub>3</sub>, whether alone or mixed with NiO or TiO<sub>2</sub>, further provide justification for performing DFT modelling using MAI to understand why degradation pathway of MAPbI<sub>3</sub> is changed when contacting with NiO, but remains the same when contacting TiO<sub>2</sub>. In the DFT calculations, we start with MAI molecule in the gas phase and compare the two possible intrinsic degradation pathways:

$$CH3NH3I(g) = HI(g) + CH3NH2(g)$$
(6)

or 
$$CH_3NH_3I(g) = NH_3(g) + CH_3I(g)$$
. (7)

The results show that MAI decomposition in the gas phase is endothermic with 64 kJ/mol and 26 kJ/mol for reaction (6) and (7), respectively. Thus, decomposition to NH<sub>3</sub> and CH<sub>3</sub>I (reaction (7)) is favored. We next analyze the changes in reaction energy on different oxide surfaces. When MAI molecules are adsorbed on the surface, the energetics change. The reactions

$$CH_3NH_3I^* = HI^* + CH_3NH_2^*$$
 (8)

or 
$$CH_3NH_3I^* = NH_3^* + CH_3I^*,$$
 (9)

where \* denotes molecules attached to surfaces, now depend on the type of oxide substrates (Figure S10). The adsorption energies of CH<sub>3</sub>NH<sub>3</sub>I, HI, CH<sub>3</sub>NH<sub>2</sub>, CH<sub>3</sub>I, and NH<sub>3</sub> and reaction energies of (8) and (9) (calculated from adsorption energies) are summarized in Table 1. The calculation results indicate that the MAI decomposition into HI + CH<sub>3</sub>NH<sub>2</sub> is favored over the NH<sub>3</sub> + CH<sub>3</sub>I pathway on NiO and TiO<sub>2</sub> surfaces. On NiO, the reaction energies of (8) and (9) are -9.35 kJ/mol and 50.8 kJ/mol, respectively (Figure 3a). Thus, the preferred degradation pathway of MAI is altered when it is adsorbed on the NiO surface. This change in the reaction pathway has profound impact on the stability of MAPbI<sub>3</sub>. Second, CH<sub>3</sub>NH<sub>2</sub> is the desorbed gas from reaction (8) because HI binding on oxide surface is much stronger (higher adsorption energy), consistent with

experiments where no HI gas is observed. On NiO, CH<sub>3</sub>I\* has the lowest adsorption energy of -47.4 kJ/mol. If reaction (9) were to occur on NiO, we would have detected CH<sub>3</sub>I in the evolved gases, which is not the case. This observation further supports the change in reaction pathway at the interface. The dissociation of HI\* to H\* on O and I\* on Ni results in the formation of H<sub>2</sub>O, which desorbs as water vapor and hence detected in both FTIR and MS, while NiI<sub>2</sub> remains as a solid by-product (Figure S11a). The lower T<sub>th</sub> when mixed with NiO than with SnO<sub>2</sub> arises from the more negative formation enthalpy of NiI<sub>2</sub> compared to SnI<sub>4</sub> (Table S3).<sup>24</sup>

**Table 1.** Adsorption energies and reaction energies on NiO (001) and TiO<sub>2</sub> (001). <sup>a)</sup> Atomic configuration of CH<sub>3</sub>NH<sub>3</sub>I\* is CH<sub>3</sub>NH<sub>2</sub>\*+H\*+I\*. <sup>b)</sup> HI\* is decomposed into H\*+I\* on NiO/TiO<sub>2</sub> surface. H and I are bonded to O and Ni/Ti, respectively.

	NiO (001) (kJ/mol)	TiO <sub>2</sub> (001) (kJ/mol)
CH <sub>3</sub> NH <sub>3</sub> I* <sup>a)</sup>	-149	-257
HI* b)	-124	-208
CH <sub>3</sub> NH <sub>2</sub> *	-95.5	-158
CH <sub>3</sub> I*	-47.4	-79.2
NH <sub>3</sub> *	-76.7	-140
$CH_3NH_3I^* = HI^* + CH_3NH_2^*$	-9.35	-44.1
$CH_3NH_3I^* = NH_3^* + CH_3I^*$	50.8	63.5

Lastly, molecular binding on TiO<sub>2</sub> is much stronger than on NiO, indicating that these molecules will remain on TiO<sub>2</sub> surface. This difference in MAI binding on NiO vs. TiO<sub>2</sub> surface arises from the presence of density of states (DOS) of MAI (green) near the valence band edge for NiO (red, Figure 3b), while the same states are deeper for TiO<sub>2</sub> (blue, Figure 3c). Hence, once a monolayer is built up on TiO<sub>2</sub>, further adsorption or reaction cannot proceed, i.e. the surface becomes inert. Thus, the only remaining degradation pathway is bulk decomposition, as shown

experimentally in Figure S8. Thus, DFT calculations provide theoretical basis for the difference in bulk vs. interfacial decomposition of MAPbI<sub>3</sub>. Furthermore, our thermal degradation studies on NiO<sub>x</sub>/MAI film (Figure S12) show that the interfacial stability is significantly lowered ( $\leq 150$  °C)

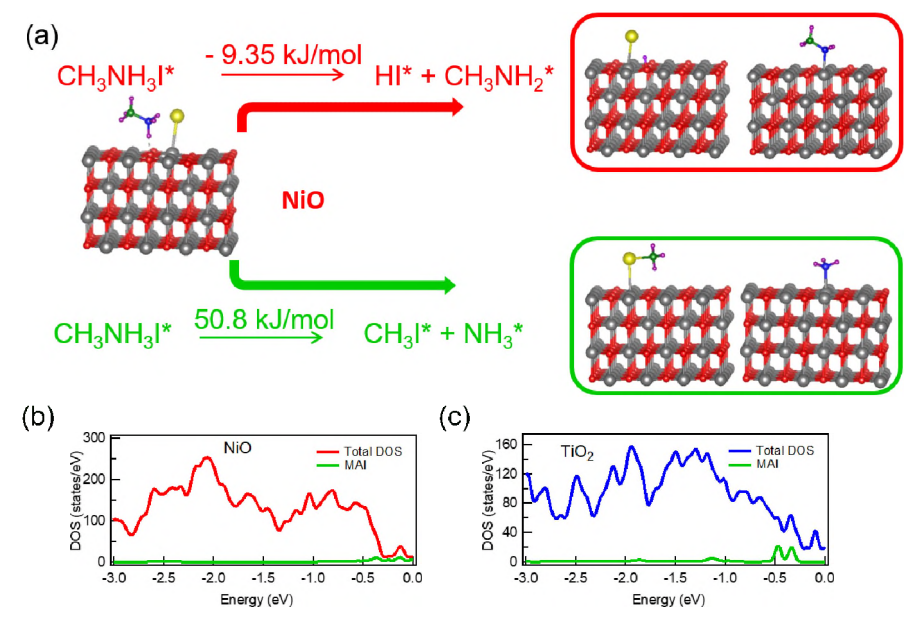


**Figure 3.** (a) Intrinsic degradation pathways of MAI on NiO surface. Upper and lower panels exhibit the degradation of MAI into HI + CH<sub>3</sub>NH<sub>2</sub> (red) and CH<sub>3</sub>I and NH<sub>3</sub> (green), respectively. Atomic configurations are obtained by the DFT calculations for the adsorption on NiO (001) surface. Pink, blue, green, yellow, grey, and red balls represent the H, N, C, I, Ni, and O atoms, respectively. DOS of MAI adsorbed on (b) NiO (red) and (c) TiO<sub>2</sub> (blue). The green lines in (b) and (c) are projected DOS of MAI.

in films compared to powder samples as films have higher surface-to-volume ratio. This result indicates that the interfacial degradation in perovskite devices could be significant at typical processing temperatures.

In summary, we show that interfacial reaction between oxide transport layers and perovskite active layer can lower the intrinsic stability of MAPbI<sub>3</sub>. DFT calculations reveal that the energetics of surface reaction favor the alternative reaction pathway. Our experimental results and thermodynamic data substantiate that the stability decreases in the following order: MAPbI<sub>3</sub>

+ TiO<sub>2</sub> ~ MAPbI<sub>3</sub> alone > MAPbI<sub>3</sub> + SnO<sub>2</sub> > MAPbI<sub>3</sub> + NiO. The interfacial degradation of

MAPbI<sub>3</sub> in contact with NiO or SnO<sub>2</sub> produces H<sub>2</sub>O and CH<sub>3</sub>NH<sub>2</sub> and occurs at lower temperature

than bulk decomposition. Similar reaction does not happen with TiO<sub>2</sub> because molecules are

strongly bound on TiO<sub>2</sub> surface, preventing further reaction. While there are other factors that can

contribute to interfacial stability, e.g. photocatalytic behavior of TiO<sub>2</sub> under UV light or charge

transfer due to work function differences, 26,27 our work focuses on the thermal stability and the

degradation pathways in devices where MAPbI<sub>3</sub> must contact other materials. Such studies will

provide guidance in pairing suitable perovskite and transport layer materials and choosing

processing conditions, critical for engineering metal halide perovskite devices with enhanced

stability. Currently interfacial modification is an active field in perovskite device research. <sup>28,29</sup> Our

approach can directly study the intrinsic stability of organic-inorganic halide perovskites in contact

with other materials as in a device and evaluate interfacial modification strategies.

ASSOCIATED CONTENT

Supporting Information Details on experiments and DFT methodology, additional TPD-MS

profiles, FTIR spectra, XRD pattern of MAPbI<sub>3</sub>, TGA-DSC curves, surface areas of powders,

Tables for NIST database of m/z associated with the gases, thermodynamic energies, and XRD

patterns of films are provided.

**AUTHOR INFORMATION** 

Email: jwhsu@utdallas.edu.

**Notes** 

The authors declare no competing financial interest.

12

### **ACKNOWLEDGMENT**

We thank D. Mitzi for bringing to our attention possible reaction between perovskite and metal oxide transport layer materials, A. Walker for discussion on electron impact ionization probabilities for different molecules, and W. Xu for help with preparation of NiO<sub>x</sub> precursor solution. This material is based upon work partially supported by the U.S. Department of Energy's Office of Energy Efficiency and Renewable Energy (EERE) under Solar Energy Technologies Office (SETO) Agreement Number DE-EE0008544. S.T. acknowledges support from UT Dallas, B.Z. acknowledges support from National Science Foundation (CBET-1916612), K.-H.H. acknowledges the support by the National R&D Program through the National Research Foundation of Korea (NRF) (NRF-2015M1A2A2055836, NRF-2018R1A2B6007888), and J.W.P.H. acknowledges support from the Texas Instruments Distinguished Chair in Nanoelectronics.

### REFERENCES

- (1) Jena, A. K.; Kulkarni, A.; Miyasaka, T. Halide Perovskite Photovoltaics: Background, Status, and Future Prospects. *Chem. Rev.* **2019**, *119*, 3036–3103.
- (2) Ahmadi, M.; Wu, T.; Bin Hu. A Review on Organic–Inorganic Halide Perovskite Photodetectors: Device Engineering and Fundamental Physics. *Adv. Mater.* **2017**, *29*, 1605242.
- Quan, L. N.; Rand, B. P.; Friend, R. H.; Mhaisalkar, S. G.; Lee, T.-W.; Sargent, E. H. Perovskites for Next-Generation Optical Sources. *Chem. Rev.* **2019**, *119*, 7444–7477.
- (4) NREL Best Research-Cell Efficiencies (accessed Dec 14, 2019).
- (5) Wang, R.; Mujahid, M.; Duan, Y.; Wang, Z.-K.; Xue, J.; Yang, Y. A Review of Perovskites Solar Cell Stability. *Adv Funct Mater* **2019**, *29*, 1808843.
- Juarez-Perez, E. J.; Hawash, Z.; Raga, S. R.; Ono, L. K.; Qi, Y. Thermal Degradation of CH<sub>3</sub>NH<sub>3</sub>PbI<sub>3</sub> perovskite Into NH<sub>3</sub> and CH<sub>3</sub>I Gases Observed by Coupled Thermogravimetry–Mass Spectrometry Analysis. *Energy Environ. Sci.* 2016, 9, 3406–3410.
- (7) Nenon, D. P.; Christians, J. A.; Wheeler, L. M.; Blackburn, J. L.; Sanehira, E. M.; Dou, B.; Olsen, M. L.; Zhu, K.; Berry, J. J.; Luther, J. M. Structural and Chemical Evolution of Methylammonium Lead Halide Perovskites During Thermal Processing from Solution. *Energy Environ. Sci.* **2016**, *9*, 2072–2082.

- (8) Ciccioli, A.; Latini, A. Thermodynamics and the Intrinsic Stability of Lead Halide Perovskites CH<sub>3</sub>NH<sub>3</sub>PbX<sub>3</sub>. *J. Phys. Chem. Lett.* **2018**, *9*, 3756–3765.
- (9) Ma, L.; Guo, D.; Li, M.; Wang, C.; Zhou, Z.; Zhao, X.; Zhang, F.; Ao, Z.; Nie, Z. Temperature-Dependent Thermal Decomposition Pathway of Organic-Inorganic Halide Perovskite Materials. *Chem. Mater.* **2019**, *31*, 8515–8522.
- (10) McLeod, J. A.; Liu, L. Prospects for Mitigating Intrinsic Organic Decomposition in Methylammonium Lead Triiodide Perovskite. *J. Phys. Chem. Lett.* **2018**, *9*, 2411–2417.
- (11) Song, Z.; Wang, C.; Phillips, A. B.; Grice, C. R.; Zhao, D.; Yu, Y.; Chen, C.; Li, C.; Yin, X.; Ellingson, R. J.; *et al.* Probing the Origins of Photodegradation in Organic–Inorganic Metal Halide Perovskites with Time-Resolved Mass Spectrometry. *Sustainable Energy Fuels* **2018**, *2*, 2460–2467.
- (12) Juarez-Perez, E. J.; Ono, L. K.; Maeda, M.; Jiang, Y.; Hawash, Z.; Qi, Y. Photodecomposition and Thermal Decomposition in Methylammonium Halide Lead Perovskites and Inferred Design Principles to Increase Photovoltaic Device Stability. *J. Mater. Chem. A* **2018**, 6, 9604-9612.
- (13) Latini, A.; Gigil, G.; Ciccioli, A. A Study on the Nature of the Thermal Decomposition of Methylammonium Lead Iodide Perovskite, CH<sub>3</sub>NH<sub>3</sub>PbI<sub>3</sub>: An Attempt to Rationalise Contradictory Experimental Results. *Sustainable Energy Fuels* **2017**, 1, 1351-1357.
- Williams, A. E.; Holliman, P. J.; Carnie, M. J.; Davies, M. L.; Worsley, D. A.; Watson, T. M. Perovskite Processing for Photovoltaics: a Spectro-Thermal Evaluation. *J. Mater. Chem. A* 2014, 2, 19338–19346.
- (15) Islam, M. B.; Yanagida, M.; Shirai, Y.; Nabetani, Y.; Miyano, K. NiO<sub>x</sub> Hole Transport Layer for Perovskite Solar Cells with Improved Stability and Reproducibility. ACS Omega 2017, 2, 2291–2299.
- Chih, Y.-K.; Wang, J.-C.; Yang, R.-T.; Liu, C.-C.; Chang, Y.-C.; Fu, Y.-S.; Lai, W.-C.; Chen, P.; Wen, T.-C.; Huang, Y.-C.; *et al.* NiO<sub>x</sub> Electrode Interlayer and CH<sub>3</sub>NH<sub>2</sub>/CH<sub>3</sub>NH<sub>3</sub>PbBr<sub>3</sub> Interface Treatment to Markedly Advance Hybrid Perovskite-Based Light-Emitting Diodes. *Adv. Mater.* **2016**, *28*, 8687–8694.
- (17) Wang, K.; Olthof, S.; Subhani, W. S.; Jiang, X.; Cao, Y.; Duan, L.; Wang, H.; Du, M.; Liu, S. F. Novel Inorganic Electron Transport Layers for Planar Perovskite Solar Cells: Progress and Prospective. *Nano Energy* **2020**, *68*, 104289.
- (18) Kerner, R. A.; Rand, B. P. Linking Chemistry at the TiO<sub>2</sub>/CH<sub>3</sub>NH<sub>3</sub>PbI<sub>3</sub> Interface to Current–Voltage Hysteresis. *J. Phys. Chem. Lett.* **2017**, *8*, 2298–2303.
- (19) Kerner, R. A.; Rand, B. P. Electrochemical and Thermal Etching of Indium Tin Oxide by Solid- State Hybrid Organic-Inorganic Perovskites. *ACS Appl. Energy Mater.* **2019**, 2, 6097–6101.
- (20) Dunlap-Shohl, W. A.; Li, T.; Mitzi, D. B. Interfacial Effects During Rapid Lamination Within MAPbI<sub>3</sub> Thin Films and Solar Cells. *ACS Appl. Energy Mater.* **2019**, *2*, 5083–5093.
- (21) Jeong, D.-N.; Lee, D.-K.; Seo, S.; Lim, S. Y.; Zhang, Y.; Shin, H.; Cheong, H.; Park, N.-G. Perovskite Cluster-Containing Solution for Scalable D-Bar Coating Toward High-Throughput Perovskite Solar Cells. ACS Energy Lett 2019, 4, 1189–1195.
- (22) NIST Chemistry WebBook (accessed Dec 14, 2019).
- Yushina, I; Rudakov, B.; Krivtsov, I; Bartashevich. Thermal Decomposition of Tetraalkylammonium Iodides. *J. Therm. Anal. Calorim.* **2014**, *118*, 425-429.

- (24) Chase, M. W. *NIST-JANAF Thermochemical Tables*; 4 Ed.; American Institute of Physics, 1998.
- (25) Jain, A.; Ong, S. P.; Hautier, G.; Chen, W.; Richards, W. D.; Dacek, S.; Cholia, S.; Gunter, D.; Skinner, D.; Ceder, G.; et al. Commentary: The Materials Project: A Materials Genome Approach to Accelerating Materials Innovation. APL Mater. 2013, 1, 011002.
- (26) Niu, G.; Li, W.; Guo, X.; Wang, L. Review of Recent Progress in Chemical Stability of Perovskite Solar Cells. *J. Mater. Chem. A* **2014**, *3*, 8970–8980.
- (27) Leijtens, T.; Eperon, G. E.; Pathak, S.; Abate, A.; Lee, M. M.; Snaith, H. J. Overcoming Ultraviolet Light Instability of Sensitized TiO<sub>2</sub> with Meso-Superstructured Organometal Tri-Halide Perovskite Solar Cells. *Nat. Commun.* **2013**, *4*, 2885.
- Yang, S.; Chen, S.; Mosconi, E.; Fang, Y.; Xiao, X.; Wang, C.; Zhou, Y.; Yu, Z.; Zhao, J.; Gao, Y.; *et al.* Stabilizing Halide Perovskite Surfaces for Solar Cell Operation with Wide-Bandgap Lead Oxysalts. *Science* **2019**, *365*, 473–478.
- (29) Kim, J.; Ho-Baillie, A.; Huang, S. Review of Novel Passivation Techniques for Efficient and Stable Perovskite Solar Cells. *Sol. RRL* **2019**, *3*, 1800302.